Deep stratospheric intrusion and Russian wildfire induce enhanced tropospheric ozone pollution over the northern Tibetan Plateau

Jinqiang Zhang [1,2,3], Dan Li[1,3,4], Jianchun Bian[1,3], Zhixuan Bai[1]

[1] Key Laboratory of Middle Atmosphere and Global Environment Observation, Institute of Atmospheric Physics, Chinese Academy of Sciences, Beijing 100029, China

[2] Collaborative Innovation Center on Forecast and Evaluation of Meteorological Disasters, Nanjing University of Information Science & Technology, Nanjing 210044, China

[3] College of Earth and Planetary Sciences, University of Chinese Academy of Sciences, Beijing 100049, China

[4] Institute of Energy and Climate Research: Stratosphere (IEK-7), Forschungszentrum Jülich, Jülich, Germany

Corresponding to: Dan Li (lidan@mail.iap.ac.cn)

Abstract: By using ozonesonde measurements, European Centre for Medium-Range Weather Forecasts (ECMWF) next-generation reanalysis ERA5 data, satellite-borne Moderate Resolution Imaging Spectrometer data products, and backward trajectory calculations from the chemical Lagrangian model of the stratosphere (CLaMS) model, this study analyzes vertical ozone distributions and explores the influence of deep stratospheric intrusions and wildfires on ozone variation in the northern Tibetan Plateau (TP) during the Asian summer monsoon period. Large ozone partial pressures were observed between 20 and 30 km, with a maximum of ~16 mPa at approximately 27 km latitude. The comparisons between the vertical ozone profiles with and without the occurrence of stratospheric intrusions showed that their relative ozone difference was up to 72.4% in the tropopause layer (15.8 km), and a secondary maximum of 66.7% existed in the middle troposphere (10.1 km). The stratospheric intrusions dried the atmosphere by 52.9% and enhanced the ozone columns by 26.1% below the upper troposphere and lower stratosphere. A case study of deep stratospheric intrusion exhibited the occurrence of large ozone partial pressure in the middle troposphere in detail, with an ozone peak of ~6 mPa at 10 km, which was caused by a tropopause fold associated with the westerly wind jet at the north flank of the Asian summer monsoon anticyclone. The stratospheric intrusion processes effectively transported the cold and dry air mass with high ozone in the stratosphere downward to the middle troposphere over the northern TP. This study also confirmed that by long-range transport processes, large wildfire smoke occurred around central and eastern Russia on 19-26 July 2016 greatly caused ozone pollution in the troposphere (6 km depth from the surface) over the northern TP.

Keywords: Enhanced tropospheric ozone, stratospheric intrusion, synoptic circulation, wildfire smoke, northern Tibetan Plateau

1. Introduction

Atmospheric ozone can regulate the amount of incoming ultraviolet radiation on the Earth's surface and is thus important for the atmospheric environment and ecosystems (Staehelin et al., 2001; Myhre et al., 2013). In the troposphere, ozone is a major greenhouse gas that primarily originates from photochemical reactions (Monks et al., 2009). Previous studies have indicated that there is an increasing trend in tropospheric ozone concentration in China, which has experienced rapid economic development and urbanization over the last few decades (Wang et al., 2012; Verstraeten et al., 2015). The increasing variation in tropospheric ozone seems to be more remarkable since the implementation of the Clean Air Action plan in 2013 in China. This plan has resulted in a significant decrease in the concentration of surface PM2.5 (particulate matter with a diameter less than 2.5 μm) as expected (Zeng et al., 2019; Zhao et al., 2020), whereas an undesirable enhancement in ozone concentration occurs in the troposphere (Xu et al., 2019; Wang et al., 2020). Currently, tropospheric ozone exacerbation has received increasing attention from Chinese scholars since it is becoming a major pollutant and is inducing complex air pollution problems (Wang et al., 2017; Ni et al., 2018). Compared with the troposphere, ozone concentration is much higher in the stratosphere where ultraviolet radiation is largely absorbed to prevent it from reaching the Earth's surface. A previous study suggested that the net infrared radiative cooling induced by CO_2 and H_2O in the stratosphere is primarily balanced by radiative heating generated from ozone absorption in ultraviolet radiation (Cañada et al., 2000).

Vertical ozone variations between the stratosphere and troposphere, i.e., transport of stratospheric ozone into the troposphere and tropospheric ozone into the lower stratosphere, have been widely deployed to study stratosphere-troposphere exchange (Dufour et al., 2015; Neu et al., 2014). By using balloon-borne measurements collected over northeastern China, a few studies have indicated that ozone-rich stratospheric air can be downward transported into the troposphere due to tropopause folding associated with cut-off low pressure systems (e.g., Li and Bian 2015; Li et al., 2015; Song et al., 2016). In addition, stratospheric intrusions can also increase ozone concentrations in the troposphere and even the boundary layer (Kuang et al., 2012; Lin et al., 2012; Li et al., 2018). Enhanced ozone concentrations in the middle troposphere have been observed by balloon measurements in the Himalayas over the southern Tibetan Plateau (TP), based on which the model simulations show that ozone-rich air masses in the stratosphere are transported to the middle troposphere to contribute to the enhanced ozone structure (Ojha et al., 2017). By analyzing 33 years of ERA-Interim reanalysis data from the European Centre for Medium-Range Weather Forecasts (ECMWF), Škerlak et al. (2014) recognized the TP as a hotspot of deep stratospheric intrusion events, where stratospheric air could be transported deep into the planetary boundary layer.

The TP is often referred to as the "roof of the world" or the "third pole of the Earth" in view of its high altitude (average elevation >4 km above sea level: ASL) and broad area (~2.5×10^6 km^2). Due to the special terrain and harsh climate, few surface observation sites exist on the TP (Zhao et al., 2020), over which ozone variation studies are mainly conducted based on satellite observations. For example, space-borne Total Ozone Mapping Spectrometer measurements have discovered a mini ozone hole during the Asian summer monsoon (ASM) period (from May-June to August-September) over the TP (Zhou et al., 1995; Zou 1996), which is very likely to harm terrestrial ecosystems and human health on the plateau (Ren et al., 1997). A limited number of studies have endeavored to collect ozonesonde measurements to illuminate the vertical ozone distributions (e.g., Shi et al., 2000; Zheng et al., 2000; Bian et al., 2012) and downward transport from the stratosphere to the troposphere induced by stratospheric intrusions (Li et al., 2018). However, such valuable studies were generally conducted over the central and southern TP, in contrast to even fewer concerns in the northern TP (Liu et al., 1997), where ozone features have not been well reported and urgently need to be better understood. Based on this consideration, we have performed ozonsonde launches over the northern TP during the ASM periods in the last three years. By using multiresource data and model simulations, this study analyzes vertical ozone variations and explores the characteristics of deep stratospheric intrusions in the northern TP. In addition, we also confirm that the wildfires that occurred around central and eastern Russia on 19-26 July 2016 had an important influence on the enhancement of tropospheric ozone pollution over the northern TP. The paper is organized as follows. The data and methods are described in Section 2. Section 3 presents the main results of the study, and a conclusion is given in Section 4.

2. Data and methods

Ozonesonde, developed by the Key Laboratory of Middle Atmosphere and Global Environment Observation at the Institute of Atmospheric Physics (IAP), Chinese Academy of Sciences (hereafter referred to as the “IAP ozonesonde”) based on an electrochemical method (Zhang et al., 2014a), was released in the northern TP during the ASM period in the last three years. IAP ozonesonde measurements have indicated reasonable reliability (Zhang et al., 2014b; Zheng et al., 2018) and have been widely used to elucidate regional ozone variations (e.g., Zhang et al., 2020; Zhou et al., 2020; Tang et al., 2021). A total of 13, 9, and 12 ozonesondes were launched at Golmud (GLM, 36.48°N, 94.93°E; 2760 m ASL) in 2016, at Qaidam (QDM; 37.74°N, 95.34°E; 3188 m ASL) in 2019, and at the QDM in 2020, respectively, over the northern TP (Fig. 1). The balloon also payloads a radiosonde to transfer observational data and detect temperature, pressure, wind field, and relative humidity (RH). The radiosonde participated in the Eighth WMO International Radiosonde Comparison and showed a reasonable performance (Nash et al., 2011), and a dry bias existed in the RH measurements above the upper troposphere and lower stratosphere (UTLS) (Bian et al., 2011). The vertical atmospheric profiles, including ozone partial pressure and the above four conventional meteorological parameters, are measured at a 1-s temporal resolution, resulting in a high vertical spatial resolution of ~5 m since the average ascent of the balloon is 5 m s^{-1}.

The Collection 6 Terra and Aqua Moderate Resolution Imaging Spectrometer (MODIS) Fire and Thermal Anomalies products are used to denote the fire points and thermal anomalies (Giglio and Justice 2015). The level 2 fire product has a 1-km spatial resolution and a daily temporal resolution. The thermal anomalies are represented as points (approximately the center of 1 km) in the data product.

The ECMWF next-generation reanalysis ERA5 data, with a horizontal resolution of 0.25°×0.25° and a temporal resolution of 1 hour (Hersbach and Dee 2016; Hoffmann et al., 2019; Li et al., 2020), are used to display the synoptic situation at high altitudes. The ERA5 reanalysis is produced by using Integrated Forecasting System (IFS) cycle 41r2 with 4-D-Var data assimilation. ERA5 is a high-resolution atmospheric dataset with a horizontal resolution of ~31 km (T_L 639 spectral grid). The data are provided on 137 hybrid sigma-pressure levels in the vertical direction from the surface to 0.01 hPa.

The Chemical Lagrangian Model of the Stratosphere (CLaMS), which has been widely employed to calculate the diabatic backward trajectory (McKenna et al., 2002, Pommrich et al., 2014), is used to explore the transport processes around the ASM anticyclone (e.g., Vogel et al., 2014, 2019; Li et al., 2017, 2018; Hanumanthu et al., 2020) for case analysis of air parcels with high ozone partial pressure in this study. The ERA5 dynamic fields with a horizontal resolution of 1°×1° and a temporal resolution of 6 hours are used to drive the trajectory model.

3. Results

3.1. Specificity of synoptic circulation and atmospheric structure over the northern TP

Figure 1 shows the mean geopotential height and wind vector at 200 hPa in August during 2016-2020 over the ASM anticyclone region. Some campaign locations, i.e., GLM, QDM, Lhasa and Kunming, also show where we launched ozonesondes during the last few years. The ASM anticyclone is a large circulation system in the UTLS that spans from the western Pacific to northern Africa during boreal summer (Bian et al., 2020). Lhasa is located at the eastern center of the ASM anticyclone, whereas Kunming is located at the southeast flank of the ASM anticyclone (Bian et al., 2012) and is influenced by the air mass from the western Pacific (Li et al., 2017) and from the inside of the ASM anticyclone. As stated in the introduction, Bian et al. (2012) used ozonesonde measurements to explore the ozone distributions over these two sites, and moreover, Li et al. (2018) reported that stratospheric intrusions can transport air masses with high ozone from high latitudes into the troposphere in Lhasa via long-range transport processes along the northeast edge of the ASM anticyclone. Compared with Kunming and Lhasa, both the GLM and QDM are located at the northern TP and are characterized by different synoptic circulations, i.e., GLM and QDM are located at the north edge of the ASM anticyclone and are also impacted by the strong westerly wind in addition to the ASM anticyclone. Given the specificity of synoptic circulations, it is reasonable to expect distinct ozone variation features at the GLM and QDM over the northern TP compared with previous literature, which is also the primary objective of this study.

The vertical distributions of atmospheric ozone, temperature and RH obtained during our campaign periods are presented in Figure 2. Large ozone partial pressure was observed between 20 and 30 km, with a maximum of ~16 mPa at approximately 27 km latitude. An annual increase tended to be indicated by ozone in the UTLS during the three years. Convective activities occurred in a few ozonesonde profiles, especially in 2016, when the air masses in the low troposphere were elevated to induce low ozone amounts (Fig. 2a) and wet air masses (Fig. 2c) in the UTLS. It has been indicated that the water vapor and ozone at the UTLS have opposite radiative forcing, i.e., the water vapor generates a cooling effect, whereas the ozone produces a heating effect by absorbing the longwave and shortwave radiations (Birner et al., 2006; Randel et al., 2007). The updrafts of ozone and water vapor in the convective conditions seemed to result in a low temperature in the UTLS (Fig. 2b). In contrast, a few ozonesonde profiles detected relatively higher ozone concentrations in the middle and low troposphere where cold and dry atmospheres existed. As explained in the following sections, these profiles are associated with 1) an intrusion of a filament of stratosphere that transports dry atmosphere with high ozone concentration downward into the troposphere and 2) Russian wildfires that transport the polluted air containing high ozone to the northern TP.

3.2. Deep stratospheric intrusions over the northern TP

The comparison of vertical averages between ozone profiles with and without stratospheric intrusions is shown in Figure 3. Higher ozone partial pressure was detected through the vertical profile when stratospheric intrusions occurred relative to their counterparts without stratospheric intrusions (Fig. 3a). The relative ozone difference was a maximum of 72.4% in the tropopause layer (15.8 km). A secondary maximum of 66.7% existed at 10.1 km. The atmospheric temperature above 20 km was generally close between the two conditions, whereas a higher temperature was detected by stratospheric intrusions between 12 and 20 km (Fig. 3b). A closer look revealed that compared with no stratospheric intrusions, the atmosphere under stratospheric intrusions was warmer by a maximum of 6.0 °C at approximately 16 km, which was consistent with the location of the maximum relative ozone difference. This significant temperature discrepancy in the UTLS should be caused by the downward transport of warm air masses from the stratosphere and ozone radiative heating effects (Birner et al., 2006; Randel et al., 2007; Kunz et al., 2009). Additionally, stratospheric intrusions can further transfer the relatively cold and dry air mass in the upper troposphere downward to the lower troposphere, leading to a colder atmospheric environment in the low and middle troposphere than those conditions without the occurrence of stratospheric intrusions. A more detailed investigation indicated that for stratospheric intrusion conditions, the subpeak of ozone at ~10 km (Fig. 3a) corresponded to a noticeable temperature variation (Fig. 3b). Relative to no stratospheric intrusions, the atmosphere was drier under stratospheric intrusions from the surface to the UTLS, with a maximum difference of >30% in the middle troposphere (Fig. 3c). To further understand the integrated influence associated with the stratospheric intrusion, the integrated ozone columns and precipitable water were also calculated from the vertical profiles below 20 km. These two calculated parameters were 47.4

DU and 1.9 cm without the occurrence of stratospheric intrusions, respectively, which were 59.8 DU and 0.9 cm when stratospheric intrusions occurred. The above values indicated that stratospheric intrusions could dry the atmosphere by 52.9% and enhance ozone columns by 26.1% below the UTLS.

Based on the above comparison, we further select typical processes to show the formation mechanism of deep stratospheric intrusion over the northern TP in detail. The vertical profiles of temperature, ozone, and RH in 2019 and 2020 at the QDM are shown in Figure 4. The temperatures on 23 July and 7 August 2019 and 23 August 2020 demonstrated a notable inverse temperature layer at ~10 km. The temperature in the middle troposphere on 23 July 2019 was clearly lower than that on the other profiles, with a maximum difference of ~10 °C at an altitude of approximately 10 km over the QDM (Fig. 4a). The ozone profiles displayed enhanced ozone partial pressure on 23 July and 7 August 2019 and 23 August 2020 (Fig. 4b), with a thickness of 1.0-1.5 km and peak values close to 6 mPa around the temperature inverse layer. The enhanced ozone layers in the middle troposphere accounted for a positive ozone anomaly (66.7%) at 10.1 km for the average profile from stratospheric intrusion events (Fig. 3a). The water vapor contents from the four profiles were generally lower than those of other profiles without ozone anomalies in the troposphere at the QDM (Fig. 4c).

The 200 hPa meteorological fields at the QDM on 22 July and 23 July 2019 are shown in Figure 5a and 5c. The center of the cut-off low pressure system was located at approximately 60°N and 90°E. QDM was located at the bottom of the low pressure system and at the north flank of the ASM anticyclone and was directly influenced by a strong northwesterly wind jet. The PV value inside the cut-off low systems was high. The pressure-latitude cross section of the potential temperature gradient passing through 62°E and the QDM showed an intense fold structure in the mid-troposphere (Figs. 5b and 5d). The 2-PVU tongue, marked as the dynamical tropopause, extended downward from 200 to 350 hPa (9–11 km), where the ozone profile showed subpeak values between 9 and 11 km on 23 July 2019 at the QDM. Most air parcels lie in the middle troposphere around the fold structure at the QDM on 23 July, while most air parcels lie in the lower stratosphere one day before. The 30-hour backward trajectory confirmed that the fold structure horizontally transported cold and dry air with high ozone from high latitudes to low latitudes (Fig. 6a-b), contributing to the low temperature and high ozone structure at the QDM on 23 July 2019. The formation mechanism for the other profiles with high ozone values in the mid-troposphere on 7 August 2019 and 23 August 2020 over the QDM (not shown) is generally similar to that on 23 July 2019. The occurrences of tropopause folding were clearly observed during the ASM period in 2019 and 2020 and induced a strong ozone-positive anomaly in the troposphere over the northern TP. Previous studies have suggested the frequent occurrence of tropopause folding along the jet and low pressure systems over the TP and Northeast China (e.g., Zhang et al., 2010; Li and Bian 2015), which is also verified in this study, as demonstrated the fact that the 2-PVU isoline of the dynamical tropopause has a fold structure between 200 hPa and 350 hPa (9–11 km) at approximately 43°N at the north edge of the jet. These findings illuminate the formation mechanism of enhanced ozone events over the northern TP characterized by distinct synoptic circulation relative to that in the above literature, which is expected to help us better comprehend the features of stratospheric intrusions based on those events detected in other mid-latitude regions (e.g., Lin et al., 2012; Li et al., 2015).

3.3. Russian wildfires induce tropospheric ozone pollution over the northern TP

Figure 7 shows the vertical profiles of temperature, ozone, and RH between 3 and 12 km in 2016 at the GLM. The temperature measurements on 25 July, 27 July and 29 July 2016 displayed a strong inverse temperature layer at 8.2, 9.0 and 7.3 km compared with the other measurements (in gray) in 2016 (Fig. 7a). Coincidentally, the ozone profiles showed a high partial pressure on 25 July, 27 July and 29 July 2016 below the temperature inverse layer (Fig. 7b). The RH variations were similar to the temperature variations, which exhibited low values against other profiles in the troposphere at the GLM (Fig. 7c). Different control processes have been proposed to explain ozone variations in the troposphere, such as photochemistry (radiation and chemistry reactions), biomass burning (Oltmans et al., 2010) and dynamic transport (Holton et al., 1995; Stevenson et al., 2013). As specified below, our results indicate that wildfire smoke and dynamic transports dominate the enhanced tropospheric ozone pollution over the northern TP during our campaign periods in 2016.

To understand the synoptic background for the high ozone partial pressure over the northern TP, the ERA5 map of geopotential height (GPH) and horizontal wind speed at 500 hPa (an altitude of approximately 6 km) on 20 July, 22 July, 23 July, and 25 July 2016 over Asia is shown in Figure 8a-d and superimposed with the backward locations of air parcels with high ozone between 6–8 km at that time. The trough over Siberia at approximately 60-90°E extended from east-northeast towards west-southwest to a maximum of 45°N and 60°E, with strong wind on the north side of the trough on 20 July at 00:00 UTC (Fig. 8a); a blocking high pressure system occurred at the north side of the trough. At this time, the air parcels with high ozone concentrations generally lie between the blocking high pressure and the trough. The GLM was located on the south side of the trough. Later, the trough moved eastward and began to decay (Fig. 8b), and air parcels moved southwestward following the east-northeast wind. On 23 July, a weak low pressure system appeared at approximately 50°N and 75°E and moved southward (Fig. 8c), which is weaker than the low pressure system at the QDM in 2019 (Fig. 5a). Air parcels moved to the bottom of the low pressure system following the weak low pressure system. On 25 July, the GLM was located on the south side of the westerly wind jet, and air parcels arrived at the GLM site.

Large wildfires occurred around central and eastern Russia during the period of 19-26 July 2016, leading to widespread smoke, as shown by the MODIS true color figure (Fig. 9a). The red dots on the map show the fires and thermal anomalies, where the fires were active on 20 July 2016. The continuously backward trajectories between 19 July and 25 July 2016 from the CLaMS model are shown to trace the source of the high ozone concentration at the GLM (Fig. 9b–c). Air parcels, originating from the central Russia boundary layer where fires occurred, were transported along the east-northeast wind (Fig. 9b) on the northwest side of the trough (as seen in Fig. 8). Then, the polluted air parcels entered the westerly wind jet on the northern TP (Fig. 9b) with weak uplift around 23 July 2016 (Fig. 9c). Two days later, the polluted air parcels from high latitudes arrived at the GLM site via long-range transport, contributing to high ozone partial pressure from the surface to 8.2 km on 25 July, and uplift processes contributed to the low temperature. Backward trajectory calculations indicated wildfires in central Russia as possible sources for the enhanced ozone partial pressure (6 km depth) in the low troposphere at the GLM on 25 July 2016. High ozone concentrations were also measured on 27 July and 29 July 2016 (Fig. 7). According to the MODIS satellite products and trajectory calculations from the CLaMS model, Russian wildfire smoke primarily accounted for the high ozone partial pressure in the troposphere over the northern TP, as shown in Figure 7. Wildfire smoke has been identified as polluting the surface ozone and vertical ozone profiles over North America (e.g., McClure and Jaffe 2018; Moeini et al., 2020). However, due to the limitations of observational samples, information on wildfire influence on vertical ozone variation is still insufficient for most parts of the world, including a large territory of China where such studies have seldom been conducted. By accidentally encountering wildfire cases during our campaign periods, we confirmed that by long-range transport processes, Russian wildfire smoke greatly caused ozone production in the troposphere (6 km depth from the surface) over the northern TP.

4. Conclusions and discussion

Accurate ozone measurements are fundamental to investigate the varying trend of ozone and its climatic and environmental effects, especially over the TP where a mini ozone hole occurs during the ASM period and ozone photochemical production is facilitated by strong ultraviolet radiation. Given the high elevation and unique geographical location of the TP, previous ozone studies have mainly focused on the analysis of total ozone columns from satellite observations. In situ vertical ozone measurements are extremely scarce over the TP, except that few atmospheric campaigns have endeavored to collect ozonesonde measurements over the central and southern TP, meaning there has been less concern in the northern TP that needs to be better reported and understood. To fill this gap, we performed 13, 9, and 12 ozonesonde launches over the northern TP during the ASM periods in 2016, 2019, and 2020, respectively. By using ozonesonde measurements, ERA5 reanalysis data, satellite-borne MODIS products and backward trajectory calculations from the CLaMS model, this study analyzes vertical ozone variations and explores the influence of deep stratospheric intrusions and wildfires on the ozone variation in the northern TP. The main findings are summarized as follows.

Large ozone partial pressure was observed between 20 and 30 km, with a maximum of ~16 mPa at approximately 27 km. An annual increasing trend was exhibited by ozone at the UTLS during our campaign periods. Deep stratospheric intrusions effectively transported dry and cold air with high ozone concentrations downward into the troposphere. The precipitable water and integrated ozone columns below the UTLS were 0.9 cm and 59.8 DU when stratospheric intrusions occurred. Compared with no stratospheric intrusions, the stratospheric intrusions dried the atmosphere by 52.9% and enhanced the ozone columns by 26.1% below the UTLS. A case study confirmed that stratospheric air with high ozone and low water vapor was transported downward to the middle troposphere at ~10 km altitude due to tropopause folds along the strong westerly wind jet associated with the cut-off low pressure system over the northern TP. Compared with previous studies focused on the UTLS region in the ASM anticyclone, this study investigated the high ozone features in the troposphere by comprehensively considering the linkage between the tropopause fold structure over the northern TP and the westerly wind jet at the northern flank of the ASM anticyclone. Moreover, by encountering Russian wildfires that occurred during our campaign periods, we originally confirmed that through long-range transport processes, wildfire smoke could greatly enhance ozone production in the troposphere (6 km depth from the surface) over the northern TP. The results in this study should be beneficial to better understand the formation mechanism of stratospheric intrusions over the TP during the ASM period, especially the influence of wildfires on ozone variation, which has rarely been reported in China. Further in situ measurements are still needed for climate research to comprehensively quantify the ozone variation in the troposphere and the boundary layer over the northern TP.

Acknowledgments

The authors would like to acknowledge Mr. Xiaowei Wan for releasing the ozonesondes in 2016 and 2020. Special thanks are extended to the Aerospace Information Research Institute, Chinese Academy of Sciences, for contributions at the QDM in 2019 and 2020. We thank the IEK-7 at Research Centre Jülich for providing the computer time. This work was supported by the Strategic Priority Research Program of the Chinese Academy of Sciences (Grant No. XDA17010101), the National Natural Science Foundation of China (Grant Nos. 41875183, 41975050 and 91837311), and the National Key R&D Program of China (Grant No. 2017YFA0603504).

Data availability

The MODIS fires and thermal anomalies are available from https://worldview.earthdata.nasa.gov (7 December 2020). The CLaMS can be downloaded from the GitLab webpage: https://jugit.fz-juelich.de/clams/CLaMS (last access: 7 December 2020) (CLaMS, 2020).

References

Bian, J., Chen, H., Vömel, H., Duan, Y., Xuan, Y., Lü, D., 2011. Intercomparison of humidity and temperature sensors: GTS1, Vaisala RS80, and CFH. *Adv. Atmos. Sci.* 28(1), 139–146. https://doi.org/10.1007/s00376-010-9170-8.

Bian, J., Pan, L., Paulik, L., Vömel, H., Chen, H., Lü, D., 2012. In situ water vapor and ozone measurements in Lhasa and Kunming during the Asian summer monsoon. *Geophys. Res. Lett.* 39, L19808. https://doi.org/10.1029/2012GL052996.

Bian, J., Li, D., Bai, Z., Li, Q., Lü, D., Zhou, X., 2020. Transport of Asian surface pollutants to the global stratosphere from the Tibetan Plateau region during the Asian summer monsoon. *Natl. Sci. Rev.* 7(3), 516–533. https://doi.org/10.1093/nsr/nwaa005.

Cañada, J., Pedrós, G., López, A., Boscá J., 2000. Influences of the clearness index for the whole spectrum and of the relative optical air mass on UV solar irradiance for two locations in the Mediterranean area, Valencia and Cordoba. *J. Geophys. Res.* 105(18), 4759–4766. https://doi.org/10.1029/1999JD901106.

Dufour, G., Eremenko, M., Cuesta, J., Doche, C., Foret, G., Beekmann, M., Cheiney, A., Wang, Y., Cai, Z., Liu, Y., Takigawa, M., Kanaya, Y., Flaud, J.-M., 2015. Springtime daily variations in lower-tropospheric ozone over east Asia: the role of cyclonic activity and pollution as observed from space with IASI. *Atmos. Chem. Phys.* 15, 10839–10856. https://doi.org/10.5194/acp-15-10839-2015.

Giglio L and Justice C 2015 MOD14 MODIS/Terra Thermal Anomalies/Fire 5-Min L2 Swath 1km V006, distributed by NASA EOSDIS Land Processes DAAC (https://doi.org/10.5067/MODIS/MOD14.006. Accessed 2020-12-17).

Hoffmann, L., Günther, G., Li, D., Stein, O., Wu, X., Griessbach, S., Heng, Y., Konopka, P., Müller, R., Vogel, B., Wright, J. S., 2019. From ERA-Interim to ERA5: the considerable impact of ECMWF's next-generation reanalysis on Lagrangian transport simulations. Atmos. Chem. Phys., 19, 3097–3124, https://doi.org/10.5194/acp-19-3097-2019.

Hersbach, H., Dee, D., 2016. ERA5 reanalysis is in production, ECMWF Newsletter 147 7 pp (available at: https://www.ecmwf. int/en/newsletter/147/news/era5-reanalysis-production)

Holton, J., Haynes, P., McIntyre, M., Douglass, A., Rood, R., Pfister, L., 1995. Stratosphere troposphere exchange. *Rev. Geophys.* 33, 403–439. https://doi.org/10.1029/95RG02097.

Kuang, S., Newchurch, M. J., Burris, J., Wang, L., Knupp, K., Huang, G., 2012. Stratosphere-to-troposphere transport revealed by ground-based lidar and ozonesonde at a midlatitude site. *J. Geophys. Res.* 117, D18305. https://doi.org/10.1029/2012JD017695.

Li, D., Bian, J., 2015. Observation of a summer tropopause fold by ozonesonde at Changchun, China: Comparison with reanalysis and model simulation. *Adv. Atmos. Sci.* 32(10), 1354–1364. https://doi.org/10.1007/s00376-015-5022-x.

Li, D., Bian, J., Fan, Q., 2015. A deep stratospheric intrusion associated with an intense cut-off low event over East Asia. *Science China: Earth Sciences,* 58, 116–128. https://doi.org/10.1007/s11430-014-4977-2.

Li, D., Vogel, B., Bian, J., Müller, R., Pan, L. L., Günther, G., Bai, Z., Li, Q., Zhang, J., Fan, Q., Vömel, H., 2017. Impact of typhoons on the composition of the upper troposphere within the Asian summer monsoon anticyclone: the SWOP campaign in Lhasa 2013.

Atmos. Chem. Phys. 17, 4657–4672. https://doi.org/10.5194/acp-17-4657-2017, 2017.

Li, D., Vogel, B., Müller, R., Bian, J., Günther, G., Li, Q., Zhang, J., Bai, Z., Vömel, H., Riese, M., 2018. High tropospheric ozone in Lhasa within the Asian summer monsoon anticyclone 2013: influence of convective transport and stratospheric intrusions. *Atmos. Chem. Phys.* 18, 17979–17994. https://doi.org/10.5194/acp-18-17979-2018.

Li, D., Vogel, B., Müller, R., Bian, J., Günther, G., Ploeger, F., Li, Q., Zhang, J., Bai, Z., Vömel, H., Riese, M., 2020. Dehydration and low ozone in the tropopause layer over the Asian monsoon caused by tropical cyclones: Lagrangian transport calculations using ERA-Interim and ERA5 reanalysis data. Atmos. Chem. Phys., 20, 4133 – 4152, https://doi.org/10.5194/acp-20-4133-2020.

Lin, M., Fiore, A.M., Cooper, O.R., Horowitz, L.W., Langford, A.O., Levy II, H., Johnson, B.J., Naik, V., Oltmans, S.J., Senff, C.J., 2012. Springtime high surface ozone events over the western United States: Quantifying the role of stratospheric intrusions. *J. Geophys. Res.* 117, D00V22. https://doi.org/10.1029/2012JD018151.

Liu, Q., Zheng, X., Luo, C., Ding, G., Li, X., Zhou, X., 1997. Ozone vertical profile characteristics over Qinghai Plateau measured by electrochemical concentration cell ozonesondes *Adv Atmos Sci.* 14(4), 481–490. https://doi.org/10.1007/s00376-997-0066-1.

Nash J, Oakley T, Vömel H and Li W 2011 WMO Intercomparison of High Quality Radiosonde Systems, Yangjiang, China, 12 July–3 August 2010. Tech. Rep. WMO, WMO/TD-No. 1580, Instruments and Observing Methods Report No. 107 (Available online: http://library.wmo.int/pmb_ged/wmo-td_1580.pdf)

Neu, J., Flury, T., Manney, G., Santee, M., Livesey, N., Worden, J., 2014. Tropospheric ozone variations governed by changes in stratospheric circulation *Nat. Geosci.* 7(5), 340–344. https://doi.org/10.1038/ngeo2138.

McClure, C., Jaffe, D., 2018. Investigation of high ozone events due to wildfire smoke in an urban area. *Atmos. Environ.* 194, 146–157. https://doi.org/10.1017/CBO9781107415324.018.

McKenna, D. S., Konopka, P., Grooß, J.-U., Günther, G., Müller, R., Spang, R., Offermann, D., Orsolini, Y., 2002. A new Chemical Lagrangian Model of the Stratosphere (CLaMS): 1. Formulation of advection and mixing. *J. Geophys. Res.* 107, ACH 15-1–ACH 15-15. https://doi.org/10.1029/2000JD000114.

Moeini, O., David. W., Tarasick, C., McElroy, T.,Liu, J., Osman, M.K., Thompson, A.M., Parrington, M., Palmer, P.I., Johnson, B., Oltmans, S.J., Merrill, J., 2020. Estimating wildfire-generated ozone over North America using ozonesonde profiles and a differential back trajectory technique. *Atmos. Environ. X***7**, 100078. https://doi.org/10.1016/j.aeaoa.2020.100078.

Monks P *et al* 2009 Atmospheric composition change–global and regional air quality *Atmos. Environ.* 43(33), 5268–5350. https://doi.org/10.1016/j.atmosenv.2009.08.021.

Myhre G *et al* 2013 Anthropogenic and Natural Radiative Forcing, in: Climate Change 2013: The Physical Science Basis. Contribution of Working Group I to the Fifth Assessment Report of the Intergovernmental Panel on Climate Change. Cambridge University Press, Cambridge, UK and New York, NY, USA (Available online: https://doi.org/10.1017/CBO9781107415324.018)

Ni, R., Lin, J., Yan, Y., Lin, W., 2018. Foreign and domestic contributions to springtime ozone over China. *Atmos. Chem. Phys.* 18, 11447–11469. https://doi.org/10.5194/acp-18-11447-2018.

Ojha, N., Pozzer, A., Akritidis, D., Lelieveld, J., 2017. Secondary ozone peaks in the troposphere over the Himalayas. *Atmos. Chem. Phys.* 17, 6743–6757. https://doi.org/10.5194/acp-17-6743-2017.

Oltmans, S.J., Lefohn, A.S., Harris, J.M., Tarasick, D.W., Thompson, A.M., Wernli, H., Johnson, B.J., Novelli, P.C., Montzka, S.A., Ray, J.D., Patrick, L.C., Sweeney, C., Jefferson, A., Dann, T., Davies, J., Shapiro, M., Holben, B.N., 2010. Enhanced ozone over western North America from biomass burning in Eurasia during April 2008 as seen in surface and profile observations. *Atmos. Environ.* 44, 4497–4509. https://doi.org/10.1016/j.atmosenv.2010.07.004.

Pommrich, R., Müller, R., Grooß, J.-U., Konopka, P., Ploeger, F., Vogel, B., Tao, M., Hoppe, C. M., Günther, G., Spelten, N., Hoffmann, L., Pumphrey, H.-C., Viciani, S., D'Amato, F., Volk, C. M., Hoor, P., Schlager, H., Riese, M., 2014. Tropical troposphere to stratosphere transport of carbon monoxide and long-lived trace species in the Chemical Lagrangian Model of the Stratosphere (CLaMS). *Geosci. Model Dev.* 7, 2895–2916. https://doi.org/10.5194/gmd-7-2895-2014, 2014.

Shi, G., Bai, Y., Iwasaka, Y., Ohashi, T., 2000. A balloon measurement of the ozone vertical distribution over Lhasa. *Advance in Earth Sciences.* 15(5), 522–524. https://doi.org/1001-8166(2000) 05-0522-03 (in Chinese)

Škerlak, B., Sprenger, M., and Wernli, H., 2014. A global climatology of stratosphere–troposphere exchange using the ERA-Interim data set from 1979 to 2011.

Atmos. Chem. Phys. 14, 913–937. https://doi.org/10.5194/acp-14-913-2014.

Song, Y., Lü, D., Li, Q., Bian, J., Wu, X., Li, D., 2016. The impact of cut-off lows on ozone in the upper troposphere and lower stratosphere over Changchun from ozonesonde observations. *Adv. Atmos. Sci.* 33(2), 135–150. https://doi.org/10.1007/s00376-015-5054-2.

Staehelin, J., Harris, N., Appenzeller, C., Eberhard, J., 2001. Ozone trends: A review. *Rev. Geophys.* 39, 231–290. https://doi.org/10.1029/1999RG000059.

Stevenson, D. S., Young, P. J., Naik, V., Lamarque, J.-F., Shindell, D. T., Voulgarakis, A., Skeie, R. B., Dalsoren, S. B., Myhre, G., Berntsen, T. K., Folberth, G. A., Rumbold, S. T., Collins, W. J., MacKenzie, I. A., Doherty, R. M., Zeng, G., van Noije, T. P. C., Strunk, A., Bergmann, D., Cameron-Smith, P., Plummer, D. A., Strode, S. A., Horowitz, L., Lee, Y. H., Szopa, S., Sudo, K., Nagashima, T., Josse, B., Cionni, I., Righi, M., Eyring, V., Conley, A., Bowman, K. W., Wild, O., Archibald, A., 2013. Tropospheric ozone changes, radiative forcing and attribution to emissions in the Atmospheric Chemistry and Climate Model Intercomparison Project (ACCMIP). *Atmos. Chem. Phys.* 13, 3063–3085. https://doi.org/10.5194/acp-13-3063-2013.

Tang, G., Liu, Y., Zhang, J., Liu, B., Li, Q., Sun, J., Wang, Y., Xuan, Y., Li, Y., Pan,J., Li, X., Wang, Y., 2021. Bypassing the NOx titration trap in ozone pollution control in Beijing. *Atmos. Res.* 249, 105333. https://doi.org/10.1016/j.atmosres.2020.105333.

Verstraeten, W., Neu, J., Williams, J., Bowman, K., Worden, J., Boersma, K., 2015. Rapid increases in tropospheric ozone production and export from China. *Nat. Geosci.* 8(9), 690–695. https://doi.org/10.1038/ngeo2493.

Vogel, B., Günther, G., Müller, R., Grooß, J.-U., Hoor, P., Krämer, M., Müller, S., Zahn, A., Riese, M., 2014. Fast transport from Southeast Asia boundary layer sources to northern Europe: rapid uplift in typhoons and eastward eddy shedding of the Asian monsoon anticyclone. *Atmos. Chem. Phys.* 14, 12745–12762. https://doi.org/10.5194/acp-14-12745-2014.

Vogel, B., Müller, R., Günther, G., Spang, R., Hanumanthu, S., Li, D., Riese, M., Stiller, G. P., 2019. Lagrangian simulations of the transport of young air masses to the top of the Asian monsoon anticyclone and into the tropical pipe. Atmos. Chem. Phys. 19, 6007 – 6034, https://doi.org/10.5194/acp-19-6007-2019.

Wang ,T., Xue, L., Brimblecombe, P., Lam, Y., Li, L., Zhang, L., 2017. Ozone pollution in China: A review of concentrations, meteorological influences, chemical precursors, and effects *Sci. Total Environ.* 575, 1582–1596. https://doi.org/10.1016/j.scitotenv.2016.10.081.

Wang, Y., Konopka, P., Liu, Y., Chen, H., Müller, R., Plöger, F., Riese, M., Cai, Z., Lü, D., 2012. Tropospheric ozone trend over Beijing from 2002–2010: ozonesonde measurements and modeling analysis. *Atmos. Chem. Phys.* 12(18), 8389–8399. https://doi.org/10.5194/acp-12-8389-2012.

Wang Y *et al* 2020 Contrasting trends of PM2.5 and surface ozone concentrations in China from 2013 to 2017 *Natl. Sci. Rev.* 7(8), 1331–1339. https://doi.org/10.1093/nsr/nwaa032.

Ren, P., Sigernes, F., Gjessing, Y., 1997. Ground-based measurements of solar ultraviolet radiation in Tibet: Preliminary results. *Geophys. Res. Lett.* 24(11), 1359−1362. https://doi.org/10.1029/97GL01319.

Xu, J., Tie, X., Gao, W., Lin, Y., Fu, Q., 2019. Measurement and model analyses of the ozone variation during 2006 to 2015 and its response to emission change in megacity Shanghai, China. *Atmos. Chem. Phys.* 19, 9017–9035. https://doi.org/10.5194/acp-19-9017-2019.

Zeng, Y., Cao, Y., Qiao, X., Seyler, B., Tang, Y., 2019. Air pollution reduction in China: recent success but great challenge for the future. *Sci. Total Environ.* 663, 329–337. https://doi.org/10.1016/j.scitotenv.2019.01.262.

Zhang, M., Tian, W., Chen, L. Lü, D., 2010. Cross-tropopause mass exchange associated with a tropopause fold event over the northeastern Tibetan Plateau. *Adv. Atmos. Sci.* 27(6), 1344–1360. https://doi.org/10.1007/s00376-010-9129-9.

Zhang, J., Xuan, Y., Yan, X. Liu, M., Tian, H., Xia, X., Pang, L., Zheng X., 2014a. Development and preliminary evaluation of a double-cell ozonesonde. *Adv. Atmos. Sci.* 31(4), 938–947. https://doi.org/10.1007/s00376-013-3104-1.

Zhang, J., Xuan, Y., Xia, X. Liu, M., Yan, X., Pang, L., Bai, Z., Wan, X., 2014b. Performance evaluation of a self-developed ozonesonde and its application in an intensive observational campaign. *Atmos. Oceanic. Sci. Lett.* **7(3),** 175–179. https://doi.org/10.3878/j.issn.1674-2834.13.0089.

Zhang, Y., Tao, M., Zhang, J., Liu, Y., Chen, H., Cai, Z., Konopka, P., 2020. Long-term variations in ozone levels in the troposphere and lower stratosphere over Beijing: observations and model simulations. *Atmos. Chem. Phys.* 20, 13343–13354. https://doi.org/10.5194/acp-20-13343-2020, 2020.

Zhao, C., Yang, Y. Fan, H., Huang, J., Fu, Y., Zhang, X., Kang, S., Cong, Z., Husi, L., Menenti, M., 2020. Aerosol characteristics and impacts on weather and climate over the Tibetan Plateau. *Natl. Sci. Rev.* 7(3), 492–495. https://doi.org/10.1093/nsr/nwz184.

Zhao, S., Yin, D., Yu, Y., Kang, S., Qin, D., Dong, L., 2020. PM2.5 and O3 pollution during 2015-2019 over 367 Chinese cities: Spatiotemporal variations, meteorological and topographical impacts. *Environ. Pollut.* 264, 114694. https://doi.org/10.1016/j.envpol.2020.114694.

Zheng, X., Xuan, Y., Lin, W., Tang, J., Tian, H., Zhang, J. Xing, Y., 2018. Performance tests and outdoor comparison observations of domestic remade ECC ozonesondes. *J. Appl. Meteor. Sci.* 29(4), 460–473. https://doi.org/10.11898/1001-7313.20180407.

Zheng, X., Tang, J., Li, W., Zhou, X., Shi, G. and Iwasaka, Y., 2000. Observational study on total ozone amount and its vertical profile over Lhasa in the summer of 1998. *J. Appl. Meteor. Sci.* 2, 173–179 (in Chinese).

Zhou, M., Wang, P., Langerock, B., Vigouroux, C., Hermans, C., Kumps, N., Wang, T., Yang, Y., Ji, D., Ran, L., Zhang, J., Xuan, Y., Chen, H., Posny, F., Duflot, V., Metzger, J.-M., De Mazière, 2020. Ground-based Fourier transform infrared (FTIR) O3 retrievals from the 3040 cm^{-1} spectral range at Xianghe, China. *Atmos. Meas. Tech.* 13, 5379–5394. https://doi.org/10.5194/amt-13-5379-2020.

Zhou, X., Luo, C., Li, W. Shi, J., 1995. Variation of total ozone over China and the Tibetan Plateau low center. *Chinese Sci. Bull.* 40(15), 1396–1398. https://doi.org/10.1360/csb1995-40-15-1396 (in Chinese).

Zou, H., 1996. Seasonal variation and trends of TOMS ozone over Tibet. *Geophys. Res. Lett.* 23(9), 1029–1032. https://doi.org/10.1029/96GL00767.

Figures

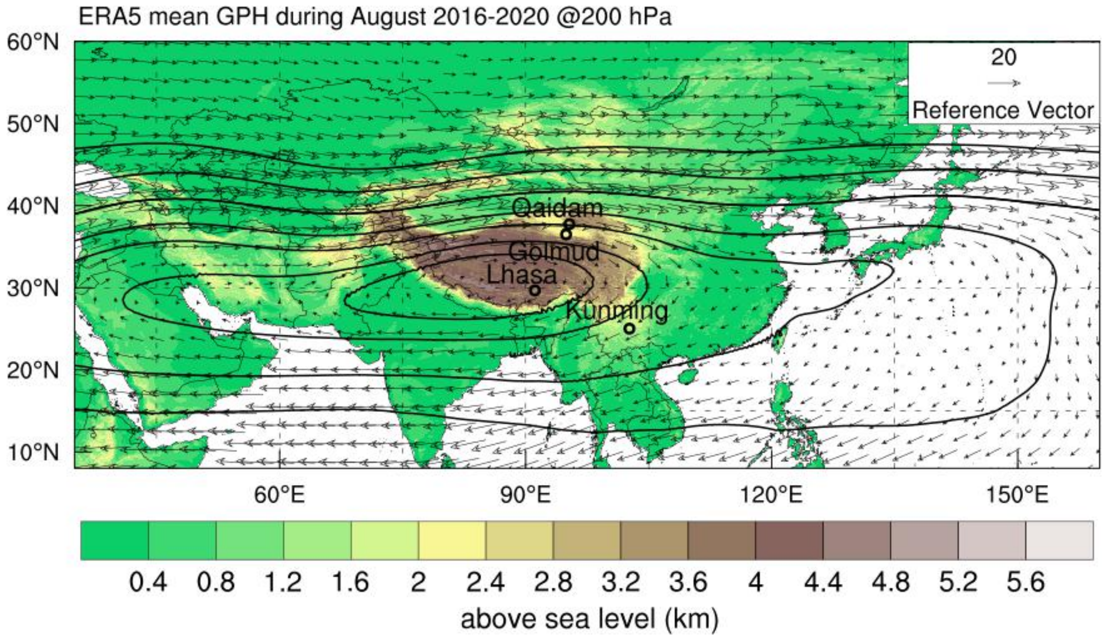

Figure 1. The ERA5 5-year (August 2016-2020) mean geopotential height (black contour) and wind vector (black arrow) at 200 hPa and campaign locations (black circles). The ground elevation (above sea level: km) is noted by the shaded area, as shown by the bottom color bar.

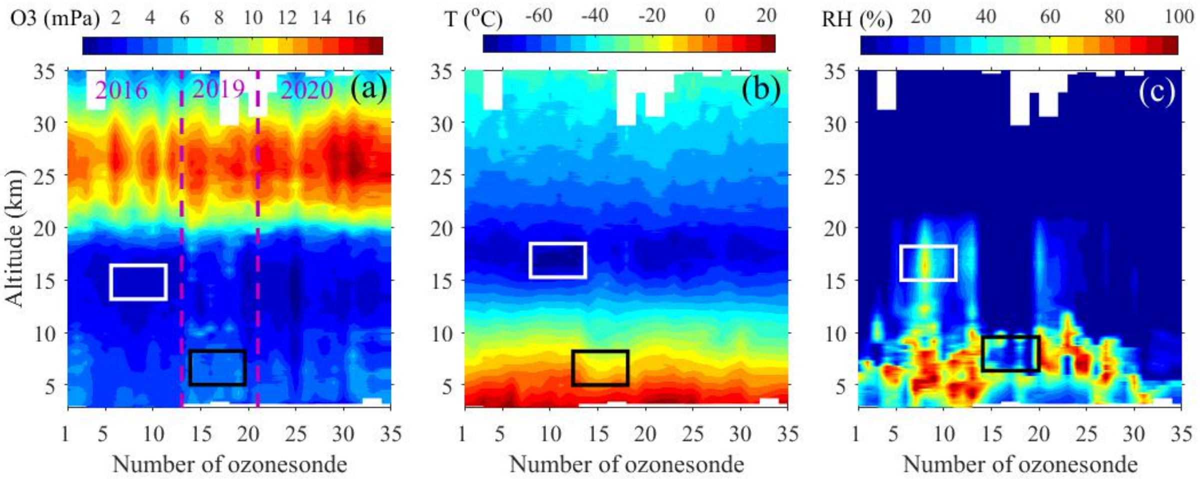

Figure 2. Vertical distributions of ozone partial pressure (a), temperature (b) and RH (c) over the northern TP in 2016, 2019 and 2020. The black rectangles denote the evident occurrence of high ozone, cold and dry air masses in the troposphere caused by deep stratospheric intrusions, whereas the white rectangles denote the wet atmospheric environment accompanied by low ozone in the UTLS associated with convective updrafts.

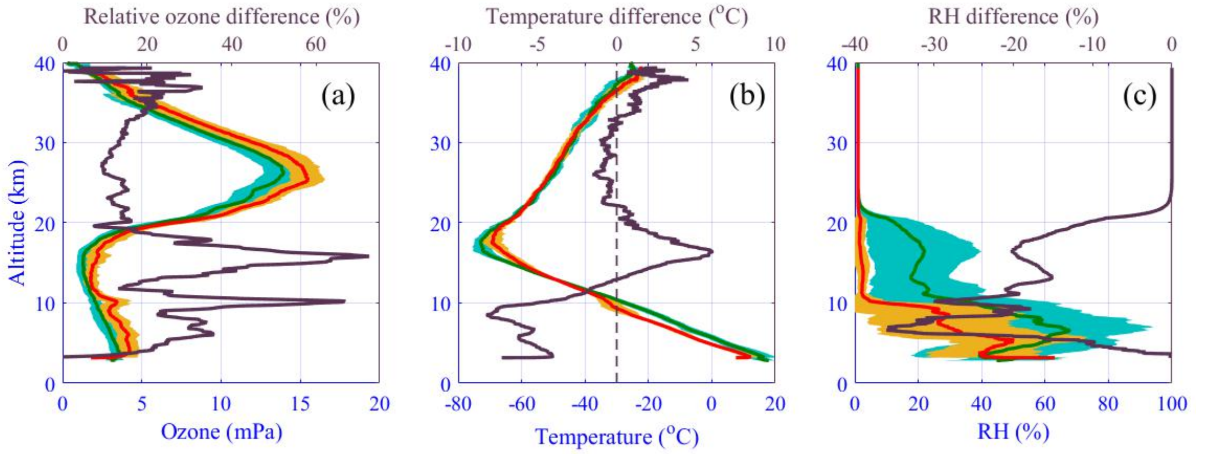

Figure 3. Comparison of vertical averages for ozone partial pressure (a), temperature (b) and RH (c) between ozonesonde profiles with (line color: red) and without (line color: green) occurrence of stratospheric intrusions. The purple lines in the three panels denote the relative ozone difference ($\frac{\text{red}-\text{green}}{\text{green}}$) and the temperature and RH differences ($\text{red} - \text{green}$), respectively.

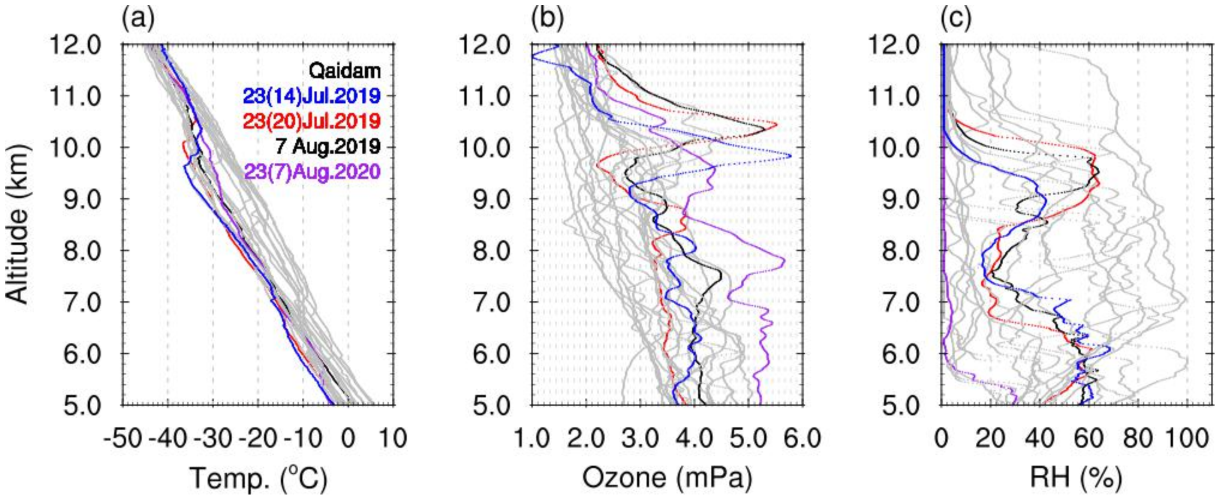

Figure 4. Vertical profiles of (a) temperature, (b) ozone partial pressure, and (c) RH in 2019 and 2020 at Qaidam, with highlights for typical stratospheric intrusions that occurred on 23 July and 7 August 2019 and 23 August 2020. The number in the bracket in the legend denotes the China standard time (in hours, UTC+8) of ozonesonde release.

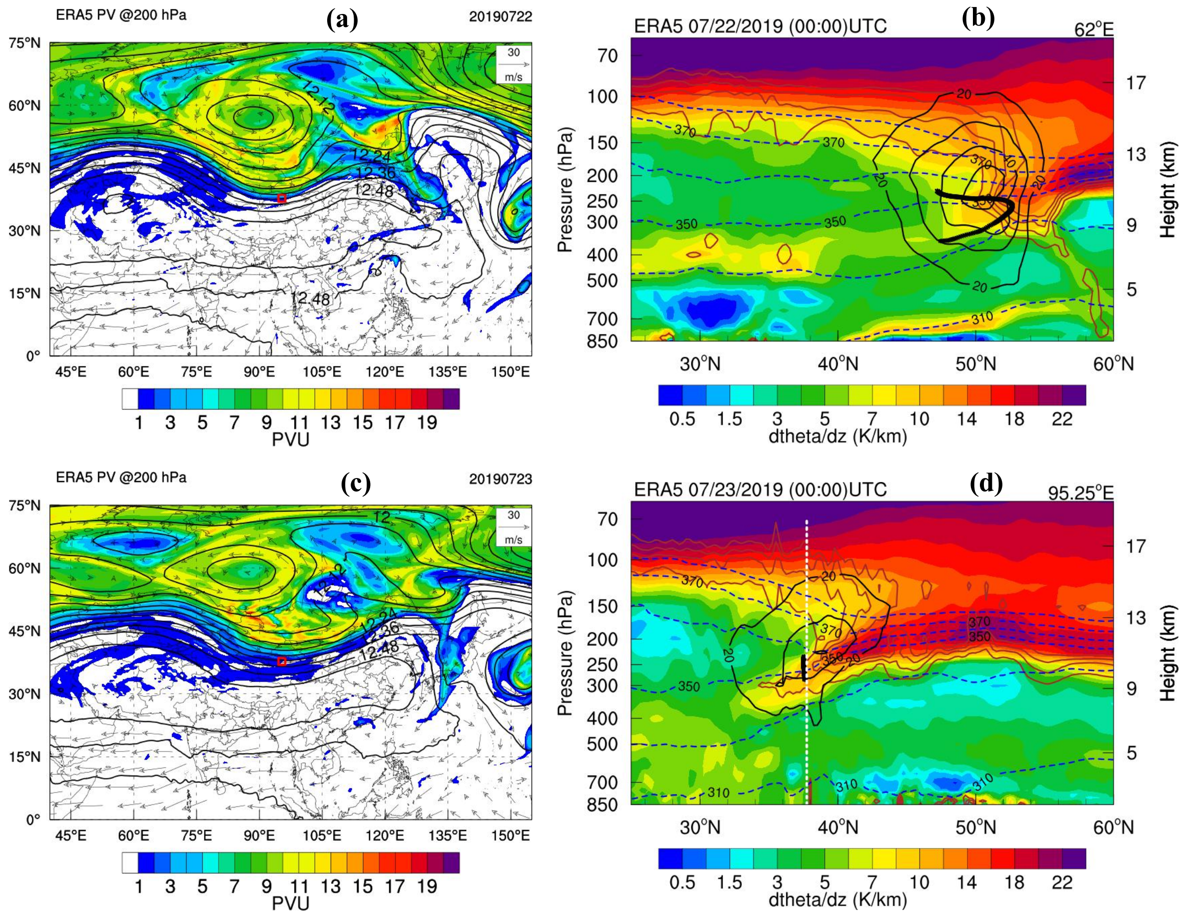

Figure 5. Left panels: the potential vorticity (1 PVU=10^{-6} m^2 s^{-1} K kg^{-1}), geopotential height (×10^3 gpm, black contours), and horizontal wind speeds (m s^{-1}, arrow) at 200 hPa on 22 July (a) and 23 July (c) 2019 at 00:00 UTC over Asia; the red square marks the location of the QDM. Right panels: the pressure-latitude cross section of the potential temperature gradient (K km^{-1}), PV (2, 4, 6, and 8 PVU, brown line), potential temperature (310 K, 330 K, 350 K, 360 K, 370 K, and 380 K, dashed line), and zonal wind (m s^{-1}, black line) at 62°E (c) and 95.25°E (d); the white vertical dashed line in (d) marks the latitude of the GLM site.

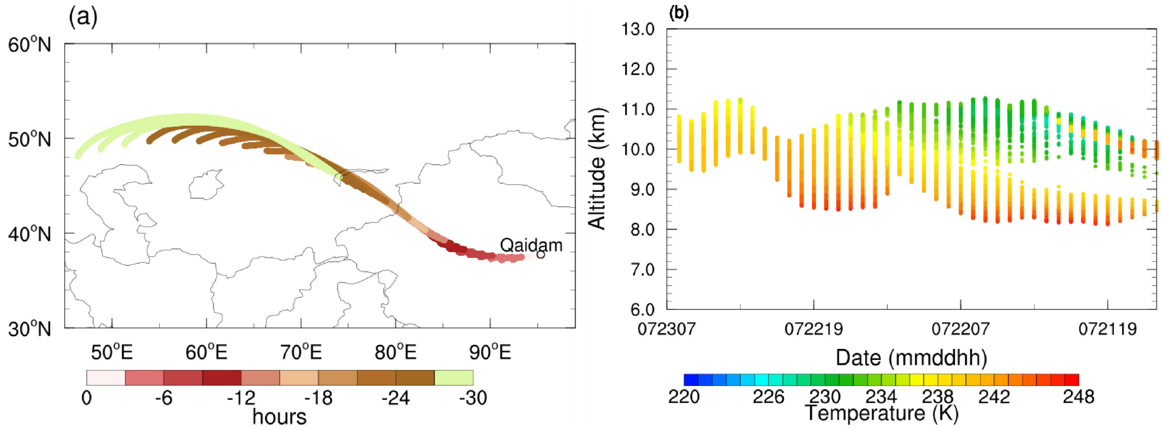

Figure 6. (a) The 30-hour backward trajectories projected on the map colored by hours. (b) Temperature as a function of altitude and date along the backward trajectories of air parcels in the altitude range of 9-11 km at Qaidam on 23 July 2019.

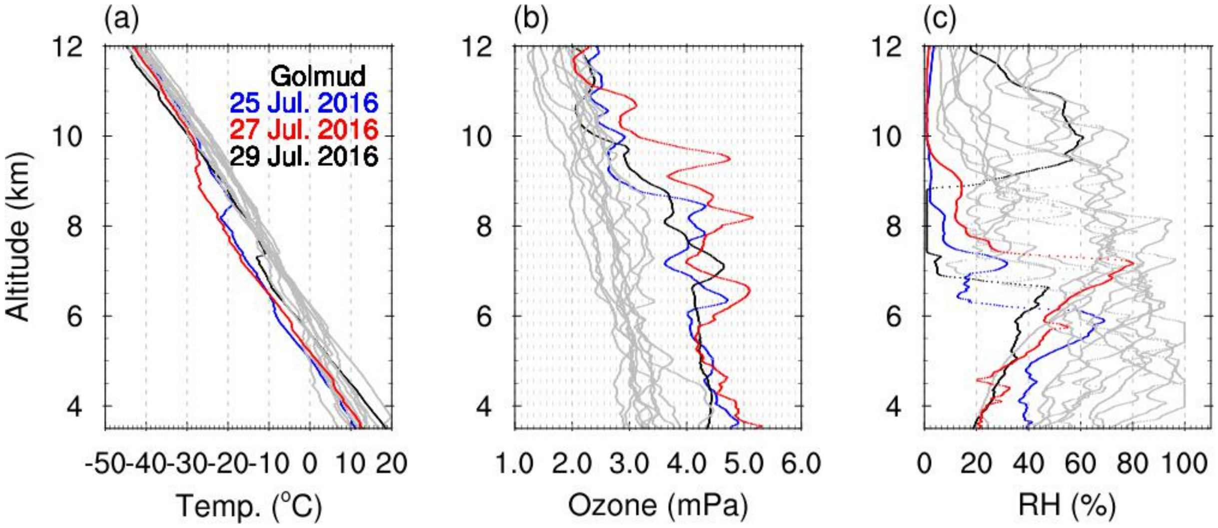

Figure 7. Vertical profiles of (a) temperature, (b) ozone partial pressure, and (c) RH in 2016 at Glomud, with highlights for Russian wildfires occurring on 25 July, 27 July, and 29 July 2016.

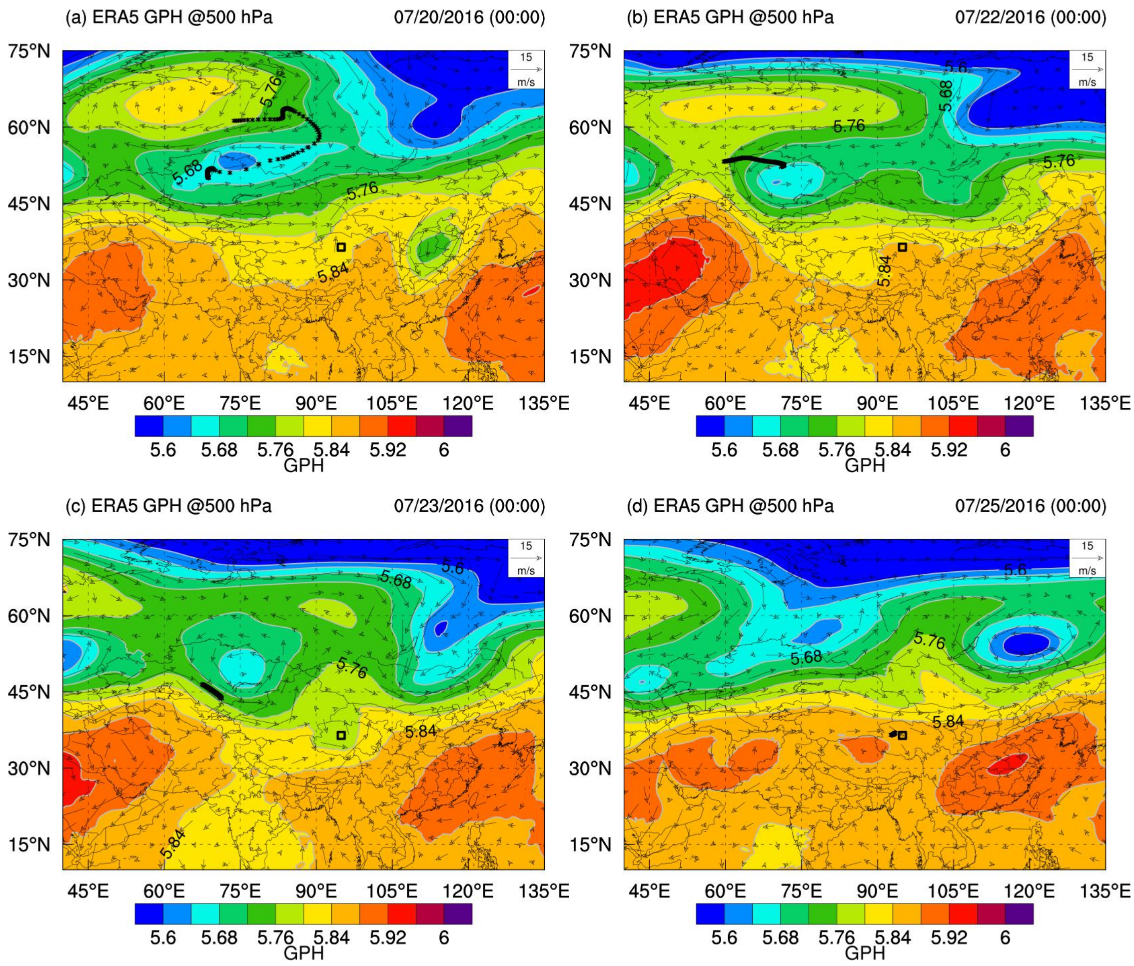

Figure 8. The geopotential height (×10^3 gpm) and horizontal wind speeds (m s^{-1}, arrow) at 500 hPa on 20 (a), 22 (b), 23 (c), and 25 (d) July 2016 at 00:00 UTC over Asia. The black square marks the location of the GLM. The asterisks mark the location of air parcels with high ozone pressure at that time.

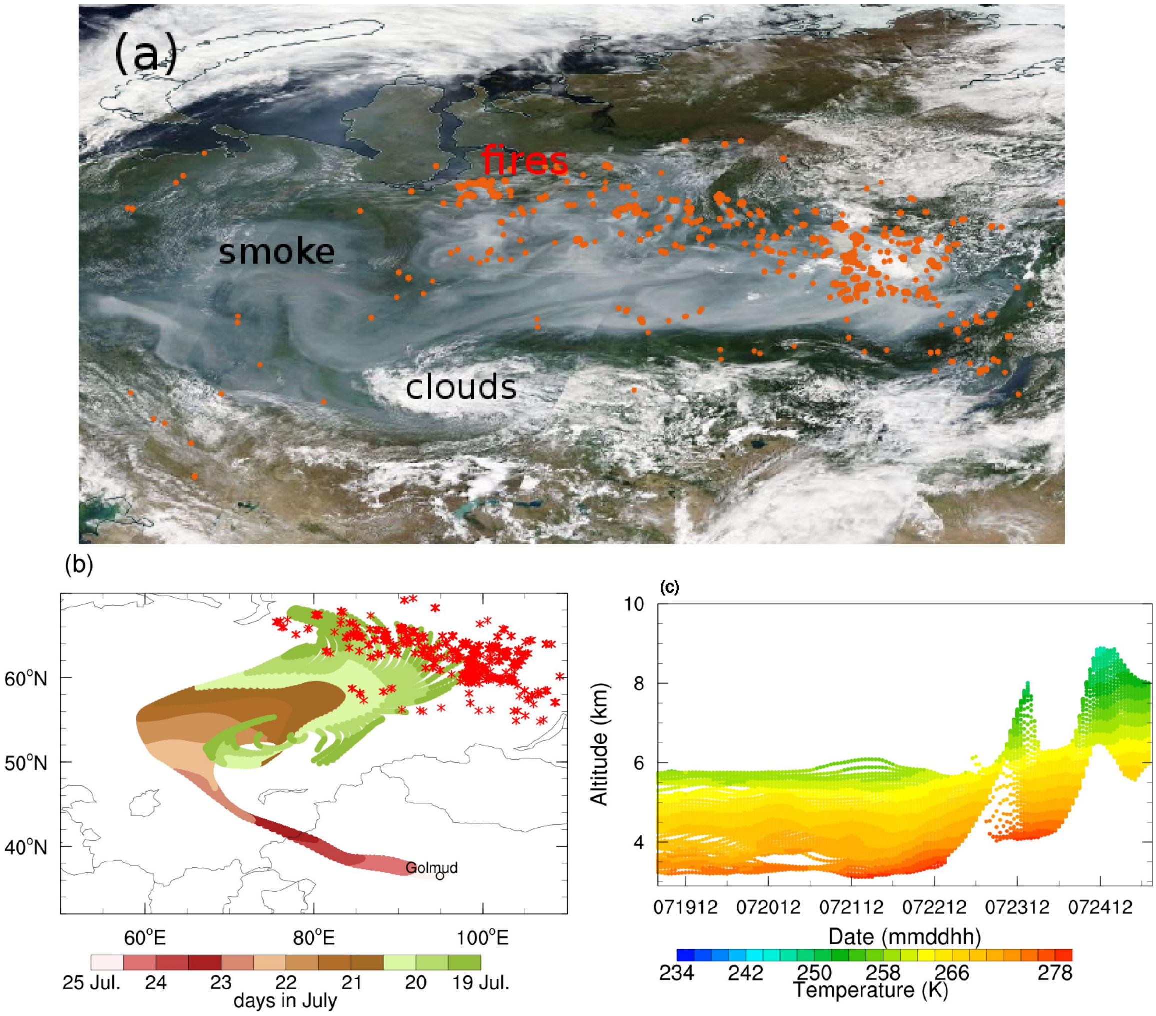

Figure 9. (a) Smoke across Russia on 20 July 2016. Red dots show fire/thermal anomalies detected by the MODIS instrument. (b) The 5-day backward trajectories projected on the map colored by days, and superimposed by fires or thermal anomalies (red asterisk) on 20 July 2016 from MODIS data. (c) Temperature as a function of altitude and date along the backward trajectories of air parcels in the altitude range of 6-8 km at the Golmud on 25 July 2016.